A repulsion mechanism explains magnesium permeation and selectivity in CorA

Olivier Dalmas, Walter Sandtner[1], David Medovoy, Ludivine Frezza, Francisco Bezanilla, and Eduardo Perozo[2]

Department of Biochemistry and Molecular Biology, Institute for Biophysical Dynamics, The University of Chicago, Chicago, IL 60637

Edited by David E. Clapham, Howard Hughes Medical Institute, Boston Children's Hospital, Boston, MA, and approved January 21, 2014 (received for review October 8, 2013)

Magnesium (Mg^{2+}) plays a central role in biology, regulating the activity of many enzymes and stabilizing the structure of key macromolecules. In bacteria, CorA is the primary source of Mg^{2+} uptake and is self-regulated by intracellular Mg^{2+}. Using a gating mutant at the divalent ion binding site, we were able to characterize CorA selectivity and permeation properties to both monovalent and divalent cations under perfused two-electrode voltage clamp. The present data demonstrate that under physiological conditions, CorA is a multioccupancy Mg^{2+}-selective channel, fully excluding monovalent cations, and Ca^{2+}, whereas in absence of Mg^{2+}, CorA is essentially nonselective, displaying only mild preference against other divalents (Ca^{2+} > Mn^{2+} > Co^{2+} > Mg^{2+} > Ni^{2+}). Selectivity against monovalent cations takes place via Mg^{2+} binding at a high-affinity site, formed by the Gly-Met-Asn signature sequence (Gly312 and Asn314) at the extracellular side of the pore. This mechanism is reminiscent of repulsion models proposed for Ca^{2+} channel selectivity despite differences in sequence and overall structure.

ion channels | electrophysiology | Mg^{2+} selectivity | AMFE

Among biological divalent cations, Mg^{2+} is not only the most abundant, but also plays an essential role in a wealth of cellular processes, including enzymatic reactions, and the stability of nucleic acids and biological membranes (1). Although the biological importance of Mg^{2+} is well established, the molecular entities and mechanisms that govern its cellular homeostasis are not well understood. In bacteria, Mg^{2+} influx is primarily catalyzed by members of the CorA family of divalent ion transport systems (2, 3). The X-ray structure of CorA has provided an excellent template toward a molecular understanding of the mechanisms underlying Mg^{2+} influx (4–7). However, although CorA has been crystallized in a wide range of conditions, so far all available CorA structures seem to correspond to nonconductive conformations, which obviously limits the basic mechanistic insights regarding Mg^{2+} selectivity and translocation that can be derived from these high-resolution structures. Computational analyses, together with NMR, X-ray absorption, and Raman spectroscopy studies, have established that Mg^{2+} holds to its first hydration shell much more tightly than any other physiological cation (8–11); this implies that any Mg^{2+}-selective transport system must either compensate for the high hydration energy (and accommodate the invariable octahedral geometry of this hexacoordinated ion) or establish a selectivity mechanism able to discriminate a hydrated or partially hydrated Mg^{2+} ion from monovalent and other divalent cations.

Several hypotheses have been postulated to explain CorA's function, including its role as a Mg^{2+}-selective channel (12), a Co^{2+} transporter (13), and even as an exporter of divalent cations (14). However, detailed mechanistic evaluation of CorA's functional properties has been limited by the resolution of existing functional assays (15). Mg^{2+} transport through CorA depends on the combination of three parameters: (*i*) number of open gates, (*ii*) the electrical potential across the membrane, and (*iii*) the Mg^{2+} driving force, none of which can be properly controlled with sufficient time-resolution in in vivo experiments. Although a prokaryotic membrane protein, we have been able to heterologously express CorA in *Xenopus* oocytes, which, in combination with standard electrophysiological approaches, allowed us to measure CorA-catalyzed divalent macroscopic currents under a variety of ionic conditions. Crystallographic studies have suggested that intracellular Mg^{2+} act as the main regulator of CorA gating under physiological conditions (6). That Mg^{2+} acts as both a gating ligand and charge carrier ultimately complicates functional studies of CorA permeation and selectivity properties. To circumvent this issue we used a mutation at the divalent cation sensor that abolishes CorA Mg^{2+}-dependent gating (Fig. 1*A*). This construct is ideally suited to evaluate ion permeation because it stabilizes steady-state currents by inhibiting the divalent ion-driven negative-feedback loop that defines CorA gating. Our results demonstrate that CorA is a bona fide multioccupancy ion channel, and that its divalent cation permeation and tight selectivity against monovalent cations can be explained on the basis of a block and repulsion mechanism, where the canonical "signature sequence" Gly-Met-Asn (GMN) plays a central role.

Results

Mg^{2+} as the Main Charge Carrier. In the presence of a negative holding potential (Vh = −60 mV), oocytes exposed to Mg^{2+}-containing solutions exhibited large inward currents under two-electrode voltage clamp (TEVC) only after being injected with CorA cRNA synthesized from a modified expression vector (Fig. 1*B*, *Left*). This Mg^{2+} inward current peaks within a few seconds (a likely reflection of the speed of the solution exchange) and

Significance

CorA is one of the major Mg^{2+} uptake systems in prokaryote, yet the mechanism of selectivity permeation is unknown. In CorA, Mg^{2+} plays a dual role of charge carrier and gating factor. Here, we use electrophysiological recordings on a CorA gating mutant to establish that Mg^{2+} selectivity arises from high-affinity divalent binding at the Gly-Met-Asn (GMN) signature motif at the extracellular loop of the channel. A repulsion mechanism through a second incoming Mg^{2+} accelerates the rate of permeation while precluding monovalent ion flux. This work establishes CorA as a multiion channel and improves our understanding of the physical properties underlying Mg^{2+} selectivity in this class of ion channels.

Author contributions: O.D., F.B., and E.P. designed research; O.D., W.S., and L.F. performed research; D.M. and L.F. contributed new reagents/analytic tools; O.D. and E.P. analyzed data; and O.D., W.S., F.B., and E.P. wrote the paper.

The authors declare no conflict of interest.

This article is a PNAS Direct Submission.

[1]Present address: Center of Physiology and Pharmacology, Medical University of Vienna, A-1090 Vienna, Austria.

[2]To whom correspondence should be addressed. E-mail: eperozo@uchicago.edu.

This article contains supporting information online at www.pnas.org/lookup/suppl/doi:10.1073/pnas.1319054111/-/DCSupplemental.

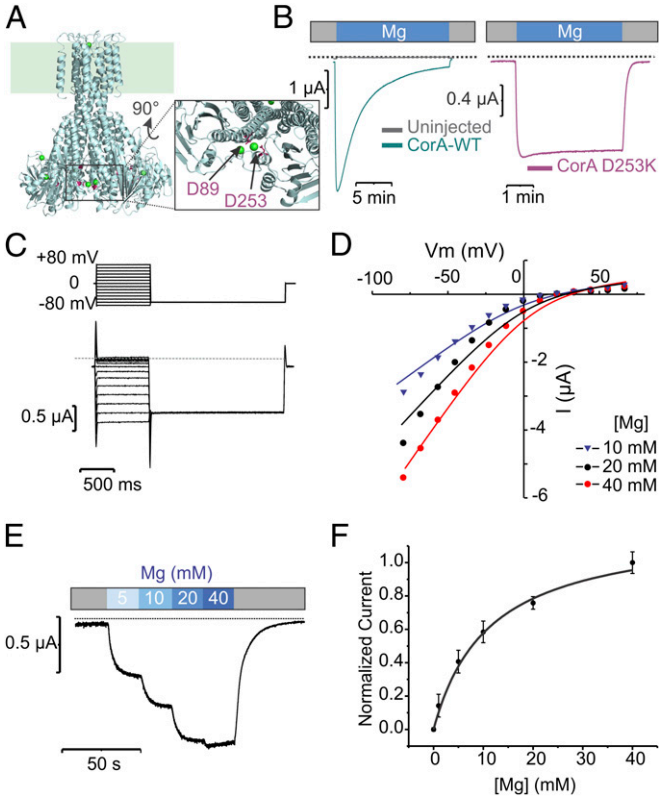

Fig. 1. CorA-driven Mg^{2+} currents recorded from TEVC. (*A*) The divalent cation sensor is highlighted on a cartoon representation of CorA crystal structure. Residues Asp89 and Asp253 are shown as purple sticks (*B*). The membrane potential (Vm) is clamped and held at −60 mV. The external solution is exchanged between two isosmotic buffers: one containing no monovalent or divalent cation (colored in gray on the horizontal bar), and one containing 20 mM Mg^{2+} (noted Mg^{2+}). A representative trace recorded on a CorA–WT-expressing oocyte is shown in teal, and control oocyte trace is shown in gray and D253K in purple. The horizontal dotted line indicates the 0 A current level. (*C*) Representative traces of CorA D253K mutant in TEVC. The voltage pulse protocol is shown on top of the current traces. The dotted line represents the 0 current levels. (*D*) The corresponding I/V relationships recorded at different external Mg^{2+} concentrations are shown. The GHK-flux equation fits are displayed as solid lines, and experimental values are dots. (*E*) Mg^{2+} current recorded at −60 mV under external solution perfusion. The external solution is changed stepwise and the corresponding solution exchange protocol is superimposed to the trace. (*F*) Mean values (±SD) of several traces ($n \geq 5$) were recorded and normalized to the maximum current. The values were plotted against the external [Mg^{2+}] and fitted with a single-site binding curve.

spontaneously decays over the course of 15–20 min to a small (less than 5% of peak) steady-state current level. This current-decay is thought to be the result of a self-regulatory gating mechanism, where accumulating cytoplasmic Mg^{2+} saturates an intracellular Mg^{2+} binding site (Fig. 1*A*), leading to channel closure. The Mg^{2+} gating site is likely formed by the pair D89, D253, located in the cytoplasmic domain (4) (Fig. 1*A*), consistent with the idea that Mg^{2+} homeostasis in bacteria takes place through a Mg^{2+} negative feedback loop (2, 6, 16). The D253K mutant displays robust steady currents but no signs of current decay (Fig. 1*B*, *Right*). Both wild-type and mutant CorA are sensitive to cobalt hexammine, a known CorA inhibitor, and are less permeable to Ni^{2+} compared with Mg^{2+} (Fig. S1); this suggests that CorA's overall permeation properties are not affected by this mutation. Hence, all subsequent experiments presented were performed using this mutation as background.

Fig. 1*C* shows a family of D253K–CorA-catalyzed Mg^{2+} currents driven at different transmembrane voltages and 20 mM external Mg^{2+}. The dependence of these inward currents on external [Mg^{2+}] can be approximated by predictions from the Goldman–Hodgkin–Katz (GHK) flux equation (*SI Materials and Methods*), assuming that Mg^{2+} is the only charge carrier (Fig. 1*D*, solid lines). All fits report an internal [Mg^{2+}] in the low millimolar range, consistent with values reported in the literature (Table S1) (17). Mg^{2+} current amplitudes at −60 mV saturate as a function of the external Mg^{2+} concentration and are best fit by a rectangular hyperbola with an apparent affinity of 11 mM (Fig. 1 *E* and *F*). This apparent K_D contrasts with larger values reported for other ion channels, such as the Shaker K^+ channel (18) but relates well with values reported for the inward rectifiers Kir1.1 and Kir2.1 (19, 20) and is consistent with the presence of a high-affinity binding-site occupancy and/or ion interactions with multiple binding sites along the long pore (21).

Cobalt Hexammine Binds to the Extracellular Mouth of the Pore. Cobalt hexammine $[Co(NH_3)_6]^{3+}$, a structural analog of hydrated Mg^{2+}, has been shown to inhibit CorA divalent influx from in vivo $^{63}Ni^{2+}$ uptake assays (22). Here, we have studied the mechanism of action of $[Co(NH_3)_6]^{3+}$ from inward current competition experiments in which we varied either $[Co(NH_3)_6]^{3+}$ or Mg^{2+} concentrations (Fig. 2 *A* and *B*). Measuring [Co $(NH_3)_6]^{3+}$ block in the presence of Mg^{2+} shows that the K_i' (apparent blocker affinity) for the blocking event shifts linearly to lower values as Mg^{2+} concentration increases, consistent with a competitive mechanism (Fig. 2*C*). The relative position of the binding site that presumably coordinates both Mg^{2+} and $[Co(NH_3)_6]^{3+}$ can be estimated from fits to the Woodhull equation (23) (*SI Materials and Methods*), which describes the

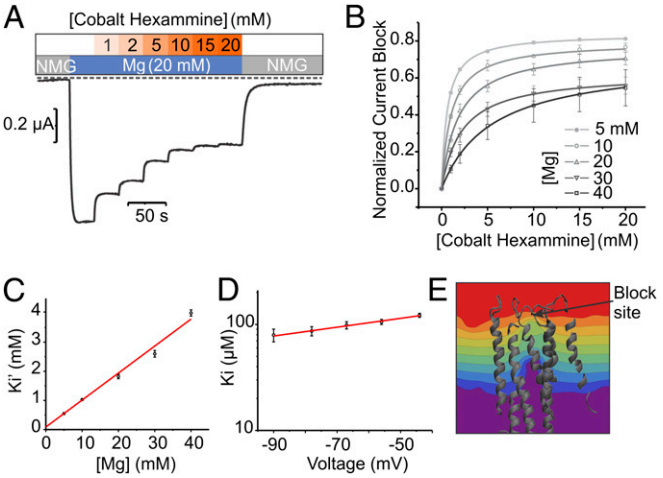

Fig. 2. Cobalt hexammine is a competitive blocker. (*A*) Under perfused TEVC setup, Mg^{2+} currents were measured at Vm = −60 mV with a stepwise increased concentration (0–20 mM) of $[Co(NH_3)_6]^{3+}$ in the presence of 20 mM $MgCl_2$. A representative current trace is superimposed with the experimental perfusion sequence. The dotted line indicates the 0 A current level. (*B*) Similar experiments were repeated at different [Mg^{2+}], and the values were fitted with one site binding to calculate the apparent blocker $[Co(NH_3)_6]^{3+}$ affinity constant (K_i'). (*C*) (K_i') were plotted against [Mg^{2+}] and fitted with the linear equation $K_i' = K_i + K_i/K_m.[Mg^{2+}]$ describing a competitive inhibition mechanism with K_i = 87 ± 28 μM and K_m = 0.9 ± 0.4 mM. (*D*) The extrapolated blocker affinity K_i were plotted in a semilog scale against the membrane potential and fitted with the Woodhull equation (23). (*E*) Close-up view of the transmembrane segments is shadowed and overlaid with the isopotential surface rainbow colored as dimensionless fractions (10% steps) of the total transmembrane potential. $[Co(NH_3)_6]^{3+}$ binding site is expected to be located in the orange/yellow section.

voltage dependence of a blocker-apparent affinity (Fig. 2*D*). The data predict a rather shallow site with an electrical distance (δ) of +0.11, placing the blocker binding site in CorA very close to the extracellular membrane–water interface (δ = 0). The structure of *Thermotoga maritima* CorA (24, 25) makes it possible to compute the transmembrane voltage profile by solving the modified Poisson–Boltzmann equation (26). A close-up view of the CorA transmembrane region and the isopotential lines map the approximate location of the blocker binding site (Fig. 2*E*). The electrical distance suggests that the $[Co(NH_3)_6]^{3+}$ binding site is located near the external end of TM1 and the extracellular TM1–TM2 loop, close to or above the signature sequence Gly-Met-Asn (GMN). Furthermore, three recent crystallographic studies show that the channel accommodates a Mg^{2+} ion by interacting with residues at the mouth of the pore (7, 24, 25), and agree with the present proposal that this binding site likely forms at least part of the Mg^{2+} selectivity filter in CorA.

Divalents Permeation Preference for CorA. The design of a Mg^{2+}-selective transport system poses a number of physical/chemical challenges in regards to its molecular mechanism of action. Mg^{2+} is the most electronegative of the biologically relevant cations, and its first shell coordination number (CN) is invariably 6, whereas for Ca^{2+} the CN can vary from 6 to 10 (27). This coordination requirement seems to be at odds with the pentameric arrangement of CorA, because coordination of a naked Mg^{2+} cannot be fully satisfied by the protein alone as it is for K^+ channels. We explored CorA permeation properties from the relative amplitude of the resulting inward current by substituting the external Mg^{2+}-containing solution to a battery of test divalent ions (Fig. 3 *A* and *B*). From these measurements, the permeability of divalent cations relative to Mg^{2+} was estimated as $Ca^{2+} > Mn^{2+} > Co^{2+} > Mg^{2+} > Ni^{2+}$ in the absence of external Mg^{2+}. Although not directly equivalent, this selectivity sequence is compatible with the idea of a high field strength site, according to a straightforward application of Coulombic interactions to a fixed, charged (or partially charged) site (28); this is in contrast to the known divalent selectivity sequence for the also pentameric acetylcholine (ACh) receptor channel (29), which parallels the sequence of ionic mobility in solution and is blocked by Ni^{2+}, Zn^{2+}, and Cd^{2+}. Tellingly, the order of the water exchange rate of these ions (30) correlates directly with the shown CorA selectivity (Fig. 3*B*), suggesting that at least a partial dehydration step is involved in the permeation process. In contrast to monovalent cations, divalents can carry two or more hydration shells in solution (31). Consequently,

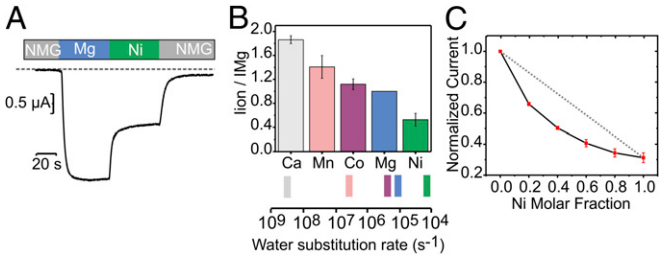

Fig. 3. The divalent cation series. (*A*) Representative trace of oocyte overexpressing CorA D253K was recorded under perfused TEVC condition with a constant membrane potential of −60 mV. The steady current values recorded in the presence of the test ion (Ni^{2+}) are used as a readout for permeation preference relative to Mg^{2+}. (*B*) Corresponding permeation ratio of divalent vs. Mg^{2+} ions. In these experiments, the divalent ion concentrations were kept even at 20 mM. The water substitution rates were adapted from Hille (30). (*C*) Normalized Mg^{2+}/Ni^{2+} steady-state currents with increasing Ni^{2+} molar fraction. The total number of divalent ions is kept constant during the experiment.

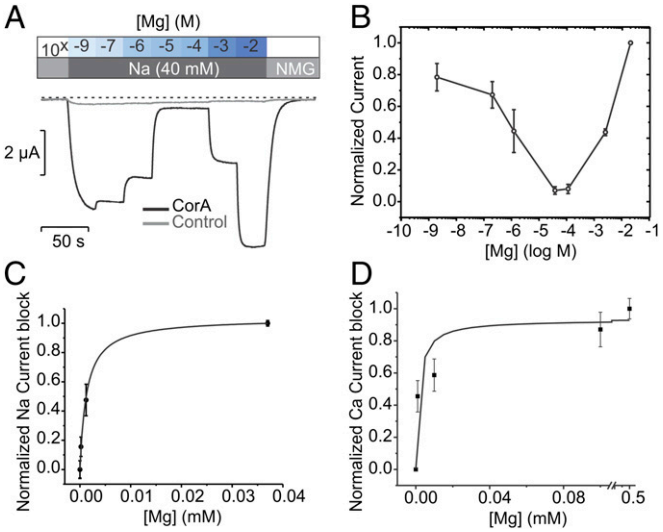

Fig. 4. CorA selectivity implies selective high-affinity binding. (*A*) Strong anomalous mole fraction effect is observed, a gradual switch in permeability from a high Na^+ permeability to a high Mg^{2+} permeability. Mg^{2+} was buffered with a mixture of EDTA/EGTA in isosmotic solutions containing a constant 40 mM [Na^+]. (*B*) The normalized current amplitudes are averaged and plotted against a log scale of the external [Mg^{2+}]. (*C*) The falling phase of the AMFE is used to calculate the affinity of CorA for Mg^{2+} for its monooccupied selective binding site. *I* is fitted with a single binding site equation $I = \frac{Im \times [Mg^{2+}]}{K_m + [Mg^{2+}]}$. The affinity is 1.3 ± 0.1 μM. (*D*) Similar experiment with 20 mM Ca^{2+} as a charge carrier. Mg^{2+} blocks Ca^{2+} current with 1.6 ± 0.8 μM affinity.

the mild selectivity observed for CorA is not suggestive of a mechanism where dehydration of the tightly bound first hydration shell is the rate-limiting step.

When the current amplitude for a test ion is plotted as a function of the molar fraction of the external solution (relative to Mg^{2+}), a clear deviation from linearity is observed (Fig. 3*C*). This phenomenon is known as the anomalous mole fraction effect (AMFE) (32, 33) and is traditionally interpreted as evidence for multiion pores under the assumption that ions are competing for similar binding sites. The presence of a robust AMFE is among the strongest pieces of evidence supporting the idea that CorA behaves as an ion channel and not as a transporter, because it suggests ions must simultaneously traverse a narrow pore in a single file, hopping from one binding site to the next (34).

CorA Selectivity Is Defined by a High-Affinity Mg^{2+} Binding Site. The mechanism through which CorA selects Mg^{2+} over Na^+ under physiological conditions has yet to be addressed. A basic approach to this issue is to evaluate the influence of Mg^{2+} on the permeability of monovalent cations at a fixed voltage. An initial glimpse of this selectivity mechanism can be obtained by measuring inward Na^+ currents (40 mM) at −60 mV in the presence of a series of Mg^{2+} concentrations. A representative trace is shown in Fig. 4*A* and points to a very strong AMFE with the presence of a relatively high-affinity divalent binding site, reminiscent of what was first observed in Ca^{2+} channels (33, 35). In the absence of Mg^{2+}, the channel is merely charge-selective and highly permeable to monovalent ions (a similar behavior was observed with K^+; Fig. S2). When small amounts of Mg^{2+} are introduced in the external solution, Na^+ currents are reduced considerably, as if Mg^{2+} binds to a blocking site with a dissociation constant of 1.3 μM ± 0.1 (Fig. 4 *B* and *C*). Thus, at trace Mg^{2+} concentrations, the Na^+ conductance is high, but as Mg^{2+} increases to micromolar concentrations, the selective region of the pore becomes occupied by a single Mg^{2+}. Because of its intimate coordination at this

binding site, the Mg^{2+} dissociation rate is much lower than it is for Na^+ (or any other monovalent cation), blocking the flow of Na^+, as expected from single-file permeation (Fig. 4*B*). A further increase in Mg^{2+} concentration leads to an almost complete block of inward currents as Mg^{2+} appears to stay bound for concentrations up to 100 μM.

Importantly, the affinity of the Mg^{2+} block effect is orders of magnitude higher than that of Mg^{2+} permeation itself (Fig. 2). The most parsimonious explanation for this phenomenon is that Mg^{2+} binding to the high-affinity "blocking" site is destabilized by the presence of other incoming Mg^{2+} in close proximity, decreasing its affinity. Indeed, when the external Mg^{2+} concentration is raised into the millimolar range, the amplitude of the inward currents increases again, producing a "rising phase" in the AMFE plot. At this higher concentration, a second Mg^{2+} can bind and, as a result of this double occupancy, the exit rate of Mg^{2+} from the pore increases. The enhancement in the Mg^{2+} off-rate is usually explained by invoking electrostatic repulsion between the two ions, but other mechanisms could also be involved (36). Regardless of the precise nature of the interaction between ions and as a result of the double occupancy, Mg^{2+} is able to flow through the channel at increasing rates dependent on the Mg^{2+} concentration.

Together with our observation of divalent–divalent interactions in the permeation pathway (AMFE; Fig. 3*C*), the presence of a dual permeability regime defined by the Mg^{2+} concentration reinforces the idea that CorA is a multisite ion channel. This behavior fits remarkably well to the repulsion model for Ca^{2+} channel selectivity, where ion discrimination depends on the presence of Ca^{2+} binding to a high-affinity site, and electrostatic repulsion secures both monovalent ion exclusion and increased throughput of divalents (32, 33). Importantly, Mg^{2+} blocks CorA-mediated Ca^{2+} currents with a remarkably similar affinity (K_D = 1.6 μM ± 0.8) as that for Na^+ currents (Fig. 4*D*). Under physiological conditions, Mg^{2+} would be present at sufficient abundance to continuously populate the high-affinity binding site, and CorA would primarily conduct Mg^{2+} without being permeable to Ca^{2+} and monovalent cations.

The GMN Signature Sequence Is Required for Ion Selectivity. In ion channels, the most conserved region of the protein is usually the key contributor to the selectivity process (37–39). Members of the CorA family of divalent-selective channels are defined by the signature sequence GMN/Met-Asn-Pro-Glu-Leu at the end of TM1 and the beginning of the extracellular loop (Fig. 5*A*; Fig. S3). Early mutagenesis studies on CorA from *Salmonella* have shown that mutating this region affects Mg^{2+} uptake (40, 41), and similar conclusions were also drawn for the yeast CorA ortholog Mrs2p (42). We have evaluated the contributions of this region to the process of Na^+/Mg^{2+} selectivity by performing alanine scanning mutagenesis between residues 309 and 323. Some of these residues cannot be mutated without a loss of expression or a loss of Mg^{2+} transport activity (Fig. 5*C*) as expected from independent mutagenesis studies (16, 43, 44). However, when Asn314 from the GMN signature sequence is mutated to Ala, the high-affinity block by Mg^{2+} is clearly compromised (Fig. 5 *B* and *C*). In contrast to the wild-type protein and all other mutants tested in this study, Na^+ currents carried out by N314A mutant are never completely blocked by Mg^{2+}. Also, increasing Mg^{2+} concentration does not produce a rising phase in the anomalous profile, which might indicate that Asn314 could be a direct contributor to the Mg^{2+} coordination site. Additionally, cobalt hexammine do not block N314A-driven Na^+ current (Fig. S4), suggesting that the selective binding site and the blocker binding site are at least partially overlapping at the GMN signature sequence. The location of this binding site is in good agreement with the mild voltage dependency (Fig. 2) as well as with recent crystallographic studies where an electron density was assigned to a Mg^{2+} coordinated by residues from the GMN signature sequence (7, 24, 25). Furthermore, mutating Gly309 or Met318 affects the Mg^{2+}/Na^+ permeation ratio in a way that leads to better Na^+ permeability than Mg^{2+}, without the influence of the Mg^{2+} block effect (Fig. 5 *B* and *C*). A plausible interpretation is that Gly309 and Met318 participate or influence a binding site physically distinct from the high-affinity one. Based on these results, we propose that the signature sequence and the N-terminal end of the extracellular loop form a multi ion selectivity filter at the extracellular mouth of CorA's permeation pathway (Fig. 5*D*). Interestingly, E316A does not critically affect either selectivity or permeation, which is in agreement with previous studies (16, 45), but clashes with our initial suggestion for the potential role of this side chain's electrostatics in Mg^{2+} selectivity (43).

On the Energetics of Mg^{2+} Binding and Coordination by CorA. Solving the Poisson–Boltzmann equation on a CorA complete structure

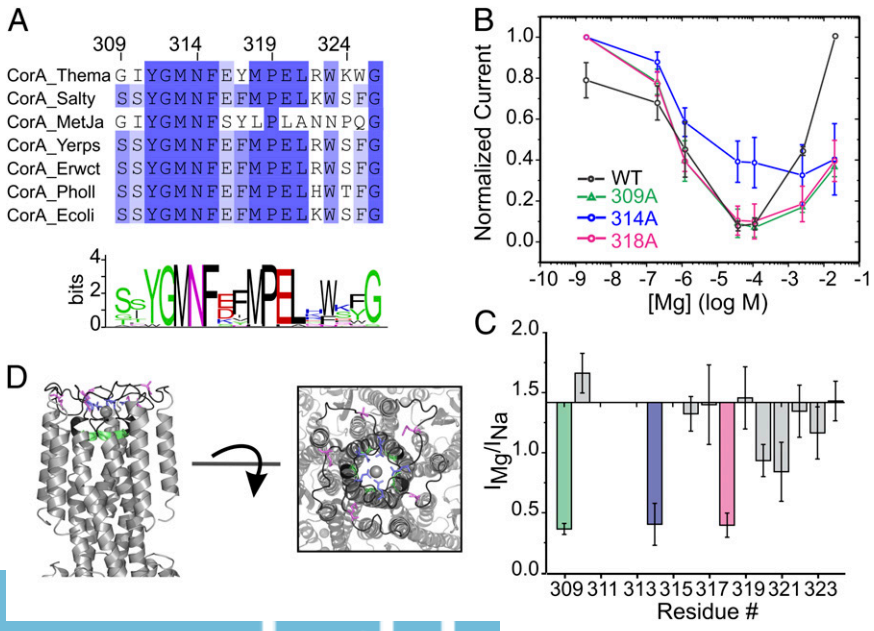

Fig. 5. The GMN motif is a molecular determinant for CorA selectivity. (*A*) Sequence alignment of CorA protein family from bacteria. For clarity, only a few sequences are displayed, and the complete sequence alignment is shown in Fig. S3. Bacteria species are labeled before each sequence for the spread of the Ala scanning mutagenesis. Sequence conservation is displayed as scaled Logo. (*B*) Mean (±SD) of normalized currents ($n \geq 5$) are plotted as a function of the Mg^{2+} concentration for the mutants with the most significant effect. The WT trace is shown in black for comparison. (*C*) The permeation preference Mg^{2+}/Na^+ is shown as a bar histogram for each individual alanine mutant. The baseline is set at the value measured for the WT channel. Mutations producing the largest effect were highlighted using the same color code as for *B*. (*D*) The mutagenized region is colored in black on the cartoon representation of the crystal structure. Mutants identified in *B* and *C* to affect Mg^{2+} selectivity are shown as sticks with the same color code.

(24) revealed a very strong electronegative surface potential, originating from the conserved residue Asn314 (from the GMN signature sequence; Fig. S5). The negatively charged pocket formed by the backbone carbonyl of Gly312 and the carboxyl group of Asn314's carboxamide seems ideally positioned to be bridged by a Mg^{2+}. The optimal spatial distribution of the carbonyls could in principle create a high-affinity binding pocket for Mg^{2+}, either through direct contact or within its first hydration shell. Given its remarkably high electronegativity, the Mg^{2+} first hydration shell is prone to favor spatially oriented water-mediated hydrogen bonds, as has been observed in B-DNA (46). It has been suggested that the Mg^{2+} bound at CorA's selectivity filter is hydrated or partially hydrated, but the moderate to low resolution of the existing crystallographic data does not allow for a definitive conclusion (7, 25). Cobalt hexammine competes with Mg^{2+} and cannot block N314A-driven currents, supporting the idea that CorA could select for a hexahydrated Mg^{2+} at the GMN motif; this has been further reinforced recently by calculations based on density functional theory (47). Lim and colleagues' theoretical framework proposes that as long as the binding pocket is large enough to accommodate a hexahydrated cation, a pentameric carbonyl configuration would be able to select Mg^{2+} over Ca^{2+}. The explanation for this selectivity resides in Mg^{2+} stronger electronegativity, leading to tighter Mg^{2+}/water/protein interactions, and is also consistent with the known degree of polarization of the water molecules in the first hydration shell (stronger than for Ca^{2+}, for instance) (47).

Discussion

Since the publication of the crystal structure of CorA from *T. maritima* by three independent research groups (4–6), the architectural uniqueness of the CorA fold and its long narrow pore have led to important, and until now unresolved, questions regarding the molecular basis of Mg^{2+} permeation and selectivity. Overexpressing CorA in *Xenopus* oocytes has eliminated an important roadblock to understand permeation, as it allowed for thorough, quantitative measurements to be made. Crystallographic evidences supported by mutagenesis studies suggest that CorA might be self-regulated by a Mg^{2+} binding site formed by Asp89 and Asp253 at the intersubunit interface (4, 6, 16). As a consequence, the time course of CorA-mediated Mg^{2+} currents would be influenced by parallel changes in the local Mg^{2+} concentrations, closing a homeostatic negative feedback loop. The inward current decay observed in oocyte is compatible with this proposal, although a clear parallel between variation in cytoplasmic Mg^{2+} concentration and current intensity await more definitive experiments. By introducing a mutations at the putative Mg^{2+} sensor we have eliminated the Mg^{2+}-dependent gating, allowing for a clear separation between gating and permeation events (Fig. 1).

The very strong electronegativity of Mg^{2+} imposes important physical/chemical challenges in the design of any Mg^{2+}-selective transport system. If Mg^{2+} is recognized and translocated with its first hydration shell intact, it would imply a selectivity process not directly linked to Mg^{2+} ionic atomic properties. However, if full dehydration is involved, it would require large amounts of energy to relieve Mg^{2+} of its hydration shell. CorA's selectivity seems to rely on a high-affinity binding of Mg^{2+} to the putative selectivity filter. Such a scenario is expected to considerably slow down permeation and to predict a small single-channel conductance (48). Interestingly, and despite repeated attempts, we were unable to measure CorA single-channel activity under conditions where macroscopic currents are readily obtained, suggesting that CorA's single-channel conductance likely operates at subpicosiemens levels under physiological conditions; this contrasts with the high conductance reported for the yeast homolog Mrs2p (49).

Experiments using mixtures of divalent ions at high (millimolar) concentrations led to the observation of an AMFE, which points to important divalent-to-divalent ion interactions within the pore (Fig. 3*C*). The AMFE is a hallmark of multiion pores and strongly supports the idea that mechanistically, CorA functions as a bona fide ion channel and not as a transporter. Mixtures of monovalent and divalent cations in a wider concentration range lead to an extreme form of AMFE, which suggests a molecular mechanism of selectivity (Fig. 4). If CorA functions as a multiion pore, and assuming the existence of at least two explicit divalent binding sites at or near the GMN selectivity filter, it is possible to describe the molecular events that lead to divalent permeation together with the exclusion of monovalent cations. In the absence of Mg^{2+}, CorA behaves as a nonselective channel freely permeable to cations. Increasing Mg^{2+} concentrations to micromolar levels tends to block nonselective cation fluxes (the "falling phase" of the AMFE in Fig. 4*B*). At millimolar Mg^{2+} levels, monovalent cation currents are fully blocked, leading to the permeation and selectivity behavior seen under physiological conditions. A high-affinity Mg^{2+} binding site is key to this selectivity mechanism where the GMN signature sequence is likely to play a central role (Fig. 5).

In agreement with recent crystallographic studies (7, 24, 25), our results point to an important role of Asn314 in Mg^{2+} coordination, possibly through its first hydration shell (47). In this scenario, Mg^{2+} permeation through the GMN selectivity filter depends upon multiple Mg^{2+} occupancy at the selectivity filter, which only becomes significant at millimolar Mg^{2+} concentrations (the rising phase of the AMFE in Fig. 4*B*). Mg^{2+} bound to its selective binding pocket plugs the channel, preventing other cations from leaking through its otherwise permissive pore. At higher concentrations, Mg^{2+} populates one or more flanking binding sites and as a consequence increases the off-rate of the blocking Mg^{2+} (likely by electrostatic repulsion) and allows for Mg^{2+} conduction. We suggest that the second Mg^{2+} binding site is located in close proximity to the Asn314 ring to allow for the electrostatic repulsion needed to secure high Mg^{2+} throughput (Fig. 6). Unfortunately, the GMN and surrounding residues are important for protein structure integrity (16, 44), and alanine substitution of residues surrounding N314 also affects CorA oocyte expression, so a direct evaluation of this hypothesis will require additional experimental evidence.

Remarkably, the present mechanism is reminiscent of what has been proposed to explain Ca^{2+} channel permeation and selectivity against monovalents (reviewed by Sather and McCleskey in ref. 50), despite any apparent structural or sequence similarity

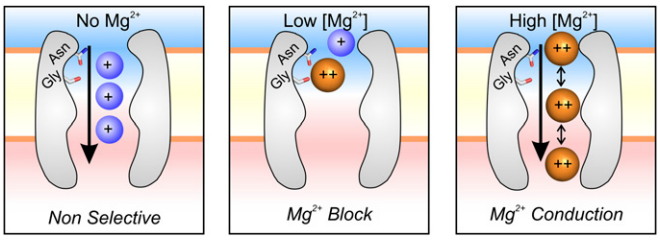

Fig. 6. Mechanism of Mg^{2+} selectivity by high-affinity binding. In the absence of Mg^{2+}, CorA is a nonselective cation channel, and cations flow down their electrochemical gradients (*Left*). CorA is able to select and bind Mg^{2+} with micromolar affinity. At this concentration, CorA is singly occupied by Mg^{2+}, which blocks the permeation pathway, producing the falling phase of the AMFE (*Center*). When [Mg^{2+}] reaches the millimolar level, additional Mg^{2+} populate lower-affinity binding sites located in the vicinity of the selective one. Proximity between charge-dense ions induces an increase of the off-rate of Mg^{2+}, likely by electrostatic repulsion (*Right*). This change in affinity leads Mg^{2+} to flow down its electrochemical gradient, the rising phase of the AMFE.

between the two classes of ion channels. We hypothesize that despite relative low sequence similarity, the basic principle described here would apply for the whole GMN divalent ion channel family. Available and upcoming structures should be evaluated in the framework of this proposed mechanism.

Materials and Methods

CorA from *Thermotoga maritima* was cloned in the pBSTA vector optimized for oocyte expression (51). Mutations were introduced by PCR using mismatch mutagenic primers as described by the Stratagene QuikChange Kit and verified by whole-gene sequencing. Oocytes were harvested from survival surgery on adult frogs according to standard protocol and injected with 50 ng of cRNA. Electrophysiology measurements were performed on a custom-made TEVC setup according to basic standard procedures (52). All experiments were reproduced on different batches of oocytes with $n > 5$, and all error bars represent SDs of the mean. The voltage dependence of the apparent blocker affinity was fitted according to the Woodhull equation (23).The electrostatic surface potential was generated by solving the Poisson–Boltzmann equation using the Adaptive Poisson–Boltzmann Solver (53) on CorA structure (24). The system was equilibrated at pH 7.0 in the presence of 300 mM ions, and the results were scaled and mapped with PyMol (54). Detailed descriptions of materials and methods are provided in *SI Materials and Methods*.

ACKNOWLEDGMENTS. We thank Prof. Luis G. Cuello and Dr. Jose S. Santos for stimulating discussion throughout the course of this work; Prof. Dirk Gillespie for enlightening feedback and experimental advice; Prof. Richard Hume for advice and use of TEVC equipment; Dr. Cédric Orelle and members of E.P.'s laboratory for critical reading of the manuscript; and Dr. H. Clark Hyde for providing assistance with curve fitting. This work was supported by National Institutes of Health Grant GM088406.

1. Maguire ME, Cowan JA (2002) Magnesium chemistry and biochemistry. *Biometals* 15(3):203–210.
2. Maguire ME (2006) Magnesium transporters: Properties, regulation and structure. *Front Biosci* 11:3149–3163.
3. Moomaw AS, Maguire ME (2008) The unique nature of mg2+ channels. *Physiology (Bethesda)* 23:275–285.
4. Lunin VV, et al. (2006) Crystal structure of the CorA Mg2+ transporter. *Nature* 440(7085):833–837.
5. Eshaghi S, et al. (2006) Crystal structure of a divalent metal ion transporter CorA at 2.9 angstrom resolution. *Science* 313(5785):354–357.
6. Payandeh J, Pai EF (2006) A structural basis for Mg2+ homeostasis and the CorA translocation cycle. *EMBO J* 25(16):3762–3773.
7. Guskov A, et al. (2012) Structural insights into the mechanisms of Mg2+ uptake, transport, and gating by CorA. *Proc Natl Acad Sci USA* 109(45):18459–18464.
8. Tongraar A, Rode BM (2005) Structural arrangement and dynamics of the hydrated Mg2+: An ab initio QM/MM molecular dynamics simulation. *Chem Phys Lett* 409(4-6): 304–309.
9. Pye CC, Rudolph WW (1998) An ab initio and Raman investigation of magnesium(II) hydration. *J Phys Chem A* 102(48):9933–9943.
10. Cappa CD, Smith JD, Messer BM, Cohen RC, Saykally RJ (2006) Effects of cations on the hydrogen bond network of liquid water: New results from X-ray absorption spectroscopy of liquid microjets. *J Phys Chem B* 110(11):5301–5309.
11. Struis RPWJ, De Bleijser J, Leyte JC (1989) Magnesium-25(2+) and chloride-35(–) quadrupolar relaxation in aqueous magnesium chloride solutions at 25.degree.C. 1. Limiting behavior for infinite dilution. *J Phys Chem* 93(23):7932–7942.
12. Maguire ME (2006) The structure of CorA: A Mg(2+)-selective channel. *Curr Opin Struct Biol* 16(4):432–438.
13. Xia Y, et al. (2011) Co2+ selectivity of *Thermotoga maritima* CorA and its inability to regulate Mg2+ homeostasis present a new class of CorA proteins. *J Biol Chem* 286(18): 16525–16532.
14. Niegowski D, Eshaghi S (2007) The CorA family: Structure and function revisited. *Cell Mol Life Sci* 64(19-20):2564–2574.
15. Romani AM (2011) Cellular magnesium homeostasis. *Arch Biochem Biophys* 512(1):1–23.
16. Payandeh J, et al. (2008) Probing structure-function relationships and gating mechanisms in the CorA Mg2+ transport system. *J Biol Chem* 283(17):11721–11733.
17. Gabriel TE, Günzel D (2007) Quantification of Mg2+ extrusion and cytosolic Mg2+-buffering in Xenopus oocytes. *Arch Biochem Biophys* 458(1):3–15.
18. Heginbotham L, MacKinnon R (1993) Conduction properties of the cloned Shaker K+ channel. *Biophys J* 65(5):2089–2096.
19. D'Avanzo N, et al. (2005) Conduction through the inward rectifier potassium channel, Kir2.1, is increased by negatively charged extracellular residues. *J Gen Physiol* 125(5): 493–503.
20. Yang L, Edvinsson J, Sackin H, Palmer LG (2012) Ion selectivity and current saturation in inward-rectifier K+ channels. *J Gen Physiol* 139(2):145–157.
21. Tao X, Avalos JL, Chen J, MacKinnon R (2009) Crystal structure of the eukaryotic strong inward-rectifier K+ channel Kir2.2 at 3.1 A resolution. *Science* 326(5960): 1668–1674.
22. Kucharski LM, Lubbe WJ, Maguire ME (2000) Cation hexaammines are selective and potent inhibitors of the CorA magnesium transport system. *J Biol Chem* 275(22): 16767–16773.
23. Woodhull AM (1973) Ionic blockage of sodium channels in nerve. *J Gen Physiol* 61(6): 687–708.
24. Nordin N, et al. (2013) Exploring the structure and function of Thermotoga maritima CorA reveals the mechanism of gating and ion selectivity in Co2+/Mg2+ transport. *Biochem J* 451(3):365–374.
25. Pfoh R, et al. (2012) Structural asymmetry in the magnesium channel CorA points to sequential allosteric regulation. *Proc Natl Acad Sci USA* 109(46):18809–18814.
26. Roux B (1997) Influence of the membrane potential on the free energy of an intrinsic protein. *Biophys J* 73(6):2980–2989.
27. Ohtaki H, Radnai T (1993) Structure and dynamics of hydrated ions. *Chem Rev* 93(3): 1157–1204.
28. Truesdell A, Christ C (1967) *Glass Electrodes for Calcium and Other Divalent Cations*, ed Eisenman G (Dekker, New York), pp 291–321.
29. Adams DJ, Dwyer TM, Hille B (1980) The permeability of endplate channels to monovalent and divalent metal cations. *J Gen Physiol* 75(5):493–510.
30. Hille B (2001) *Ion Channels of Excitable Membrane*s (Sinauer, Sunderland, MA), 3rd Ed.
31. Waluyo I, et al. (2011) The structure of water in the hydration shell of cations from X-ray Raman and small angle X-ray scattering measurements. *J Chem Phys* 134(6): 064513.
32. Almers W, McCleskey EW (1984) Non-selective conductance in calcium channels of frog muscle: Calcium selectivity in a single-file pore. *J Physiol* 353:585–608.
33. Hess P, Tsien RW (1984) Mechanism of ion permeation through calcium channels. *Nature* 309(5967):453–456.
34. Eisenman G, Latorre R, Miller C (1986) Multi-ion conduction and selectivity in the high-conductance Ca++-activated K+ channel from skeletal muscle. *Biophys J* 50(6): 1025–1034.
35. Almers W, McCleskey EW, Palade PT (1984) A non-selective cation conductance in frog muscle membrane blocked by micromolar external calcium ions. *J Physiol* 353: 565–583.
36. Miller C (1999) Ionic hopping defended. *J Gen Physiol* 113(6):783–787.
37. Heginbotham L, Lu Z, Abramson T, MacKinnon R (1994) Mutations in the K+ channel signature sequence. *Biophys J* 66(4):1061–1067.
38. Yang J, Ellinor PT, Sather WA, Zhang JF, Tsien RW (1993) Molecular determinants of Ca2+ selectivity and ion permeation in L-type Ca2+ channels. *Nature* 366(6451): 158–161.
39. Ren D, et al. (2001) A prokaryotic voltage-gated sodium channel. *Science* 294(5550): 2372–2375.
40. Szegedy MA, Maguire ME (1999) The CorA Mg(2+) transport protein of *Salmonella typhimurium*. Mutagenesis of conserved residues in the second membrane domain. *J Biol Chem* 274(52):36973–36979.
41. Smith RL, et al. (1998) The CorA Mg2+ transport protein of *Salmonella typhimurium*. Mutagenesis of conserved residues in the third membrane domain identifies a Mg2+ pore. *J Biol Chem* 273(44):28663–28669.
42. Sponder G, et al. (2013) The G-M-N motif determines ion selectivity in the yeast magnesium channel Mrs2p. *Metallomics* 5(6):745–752.
43. Dalmas O, et al. (2010) Structural dynamics of the magnesium-bound conformation of CorA in a lipid bilayer. *Structure* 18(7):868–878.
44. Palombo I, Daley DO, Rapp M (2012) The periplasmic loop provides stability to the open state of the CorA magnesium channel. *J Biol Chem* 287(33):27547–27555.
45. Moomaw AS, Maguire ME (2010) Cation selectivity by the CorA Mg2+ channel requires a fully hydrated cation. *Biochemistry* 49(29):5998–6008.
46. Guéroult M, Boittin O, Mauffret O, Etchebest C, Hartmann B (2012) Mg2+ in the major groove modulates B-DNA structure and dynamics. *PLoS ONE* 7(7):e41704.
47. Dudev T, Lim C (2013) Importance of metal hydration on the selectivity of Mg2+ versus Ca2+ in magnesium ion channels. *J Am Chem Soc* 135(45):17200–17208.
48. Bezanilla F, Armstrong CM (1972) Negative conductance caused by entry of sodium and cesium ions into the potassium channels of squid axons. *J Gen Physiol* 60(5): 588–608.
49. Schindl R, Weghuber J, Romanin C, Schweyen RJ (2007) Mrs2p forms a high conductance Mg2+ selective channel in mitochondria. *Biophys J* 93(11):3872–3883.
50. Sather WA, McCleskey EW (2003) Permeation and selectivity in calcium channels. *Annu Rev Physiol* 65:133–159.
51. Starace DM, Stefani E, Bezanilla F (1997) Voltage-dependent proton transport by the voltage sensor of the Shaker K+ channel. *Neuron* 19(6):1319–1327.
52. Dascal N (2001) Voltage clamp recordings from *Xenopus* oocytes. *Curr Protoc Neurosci* Chapter 6:12.
53. Baker NA, Sept D, Joseph S, Holst MJ, McCammon JA (2001) Electrostatics of nanosystems: Application to microtubules and the ribosome. *Proc Natl Acad Sci USA* 98(18): 10037–10041.
54. DeLano WL (2002) *The PyMol Molecular Graphics System* (DeLano Scientific, Palo Alto, CA).